KCl-Induced Corrosion of an FeCrAl Alloy at 600 °C in O_2 + H_2O Environment: The Effect of Pre-oxidation

**N. Israelsson · J. Engkvist · K. Hellström ·
M. Halvarsson · J.-E. Svensson · L.-G. Johansson**

Abstract   The present study investigates the influence of H_2O and KCl on the high temperature corrosion of an FeCrAl alloy at 600 °C. Polished samples were exposed to O_2 or O_2 + H_2O and to O_2 + H_2O with KCl applied. The samples were investigated using SEM/EDX, XRD, IC, AES and SIMS. It was found that KCl accelerates corrosion and that a rapidly growing iron-rich oxide forms with time. Chromate formation is shown to initiate the formation of a non-protective oxide scale. Pre-oxidising the alloy before exposure in the presence of KCl had a strongly beneficial effect on the corrosion.

Introduction

The constant strive for improved efficiency and lower-cost industrial processes often results in progressively higher temperatures and more aggressive environments. High temperature corrosion is a well-known problem in several industrial applications and is one of the obstacles to overcome in achieving a more sustainable society. During the past decade development has moved towards lowering fossil fuel dependency, and renewable fuels, such as biomass and waste, have become attractive options to fossil fuel for power production.

N. Israelsson (✉) · J. Engkvist · K. Hellström · J.-E. Svensson · L.-G. Johansson
Department of Environmental Inorganic Chemistry, High Temperature Corrosion Centre, Chalmers University of Technology, 412 96 Göteborg, Sweden
e-mail: niklas.israelsson@chalmers.se

M. Halvarsson
Department of Applied Physics, High Temperature Corrosion Centre, Chalmers University of Technology, 412 96 Göteborg, Sweden

The superheaters in biomass and waste-fired boilers are subject to severe corrosion attack. This is due to an aggressive environment that contains e.g. alkali salts and water combined with metal temperatures up to ∼550 °C [1–9]. At such relatively low temperatures, chromia-forming alloys, such as FeCr and FeCrNi steels, are currently being used [10]. Previous research has shown that a protective chromia scale reacts with water and oxygen to form $CrO_2(OH)_2(g)$ even at these rather low temperatures [11]. Chromia may also react to form alkali chomates in the presence of alkali salt, water and oxygen, which depletes the chromium in the oxide scale causing a non-protective iron oxide to be formed [12, 13]. These findings motivate developing new materials that are more resistant to such environments. There is also a need to increase the steam temperature in order to increase the efficiency of power plants. A limiting factor at higher temperatures is the limited lifetime of the materials due to corrosion attack.

One possible solution to the problem is to use FeCrAl alloys to lower alkali- and water vapour-induced corrosion. These materials typically consist of a ferritic iron base with 20–23 wt% Cr and 5 wt% Al. Small amounts of reactive elements (REs) such as yttrium, zirconium and hafnium can also be added to improve oxidation resistance. The advantage of this type of alloy is that a protective α-Al_2O_3 film is produced when the material is exposed to higher temperatures. α-Al_2O_3 does not suffer from evaporation and the ionic diffusivity is lower than in Cr_2O_3 [14]. These properties result in this type of material being favourable at higher temperatures, typically in the range of 900–1,300 °C.

The behaviour of FeCrAl alloys is well known at temperatures around 1,000 °C, but research at temperatures below 800 °C is limited. However there is evidence that α-Al_2O_3 forms after exposure at 700 °C in dry air after 168 and 500 h of exposure for three different FeCrAl alloys with various aluminium contents [15, 16]. Li et al. conducted an oxidation study on an FeCrAl alloy at 650 °C in static air together with KCl [17]. That investigation showed promising results for the FeCrAl alloy compared to standard stainless steels.

The present study investigates the effect of water vapour and KCl on the isothermal oxidation of an FeCrAl alloy (Kanthal® APMT) at 600 °C. Since an exclusive α-Al_2O_3 scale may not form at 600 °C, samples pre-oxidized at 700 °C were also tested to determine if pre-oxidation has a beneficial effect on corrosion. The exposed specimens were analysed using several analytical techniques.

Experimental Procedures

Material and Preparation

The commercial FeCrAl alloy Kanthal® APMT was investigated in the present study. The nominal chemical composition is given in Table 1. Sandvik Heating Technology supplied the rapidly solidified powder (RSP) material with refractory inclusions of oxides, carbides and nitrides homogeneously dispersed throughout the FeCrAl matrix. The RSP material was produced by hot isostatic pressing (HIP) of gas-atomized FeCrAl powder [18]. In addition to the main alloying elements the

material also contains minor amounts of reactive elements (RE) e.g. Y, Zr and Hf. Particles rich in RE are shown as bright spots in the backscattered electron (BSE) micrograph in Fig. 1. The material was cut into coupons with the dimensions $15 \times 15 \times 2$ mm^3 and $10 \times 8 \times 2$ mm^3. The coupons were then grounded with 320 grit SiC paper and polished in three steps using a 9, 3 and 1 μm diamond suspension. The polished coupons were degreased and cleaned using ultrasonic agitation in water, acetone and ethanol. The polished samples were dried with flowing air (~ 35 °C).

A saturated solution of KCl in water/ethanol was used to add KCl to the sample surface prior to exposure. The specimen was alternately sprayed with the solution and dried with flowing air (~ 35 °C) to avoid the formation of large droplets. The samples with 0.1 mg/cm^2 KCl were then allowed to stabilize in a desiccator before recording their weight on a six-decimal Sartorius balance. The typical size of the KCl crystals was 10–100 μm.

Exposures

Four different isothermal exposure series where carried out; the first in an environment of O_2 (10 ppm H_2O), the second in an environment of $O_2 + H_2O$, the third and fourth in an environment of $O_2 + H_2O + KCl$. The exposures were carried out in a horizontal tube furnace with 5 % O_2 or 5 % $O_2 + 40$ % H_2O balanced with nitrogen at 600 °C. Two exposures were performed at each exposure time with three samples in each experiment. The samples were mounted vertically on an alumina sample holder. The samples were placed parallel to the gas flow (1,000 ml/min which corresponds to 3.2 cm/s) to avoid interaction. The system was equipped with a humidifier producing the desired gas mixture. The samples without KCl were exposed for 24, 72 and 168 h. To investigate the effect of KCl and water vapour, the KCl-sprayed samples were exposed for 1, 9, 24, 72 and 168 h. Finally the effect of pre-oxidising the material before applying KCl was studied, and the pre-oxidation was performed in an environment of 20 % $O_2 + 80$ % N_2 at 700 °C for 24 h.

Analytical Techniques

X-ray Diffraction, XRD

A Siemens D5000 powder diffractometer was used to determine the crystalline corrosion products. The instrument was equipped with a grazing-incidence-beam attachment together with a Göbel mirror. The sample was exposed to a source of CuK$_\alpha$ radiation ($\lambda = 1.5418$ Å) with an incident angle of 0.5°. The moving detector collected data in the range of $20° < 2\theta < 60°$ with a step size of 0.05°. Silicon powder was added to the sample surface for calibration. The background was subtracted from the diffraction measurements.

Table 1 Chemical composition of Kanthal® APMT

Element	Cr	Al	Mo	Mn	Si	C	Fe	RE
wt%	21.0	5.0	3.0	≤ 0.4	≤ 0.7	≤ 0.08	bal.	Y, Zr, Hf, Ti
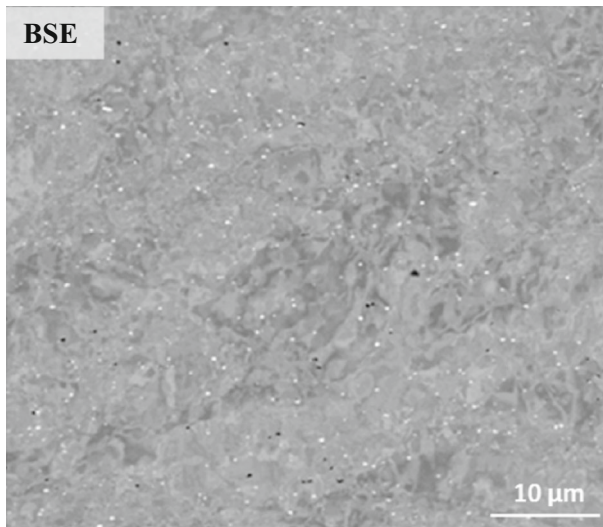
Fig. 1 BSE image of unexposed polished material

Thermo Gravimetric Analysis, TGA

A Setaram TAG thermobalance was used to study the oxidation kinetics at 600 °C in 5 % O_2 + 95 % N_2 and 5 % O_2 + 40 % H_2O + 55 % N_2 for up to 168 h. The system was equipped with a similar humidifying system as used in the horizontal tube furnace exposures. The flow rate was 15 ml/min, which corresponds to 0.3 cm/s. An alumina reference sample with the same geometry as the exposed sample ($10 \times 8 \times 2$ mm^3) was used to diminish the buoyancy effect. In addition, ex situ weight gains were recorded using a six-decimal Sartorius balance. The data were plotted from the time when the isothermal exposure temperature was reached. The time to reach 600 °C was about 6 min.

Ion Chromatography, IC

A Dionex ICS-90 system was used to establish the amount of water-soluble anions (CrO_4^{2-}, Cl^-) on the sample surface after exposure. The anions were analysed with an IonPac AS4A-SC analytic column and 1.8 mM Na_2CO_3/1.7 mM $NaHCO_3$ as the elution. The samples were also analysed with a Dionex ICS-900 system with an IonPac CS12A analytic column to determine the remaining amount of water-soluble cations (K^+). The samples were leached in 5 ml Milli-Q water using ultrasonic

agitation for 10 + 10 min. The elution was 20 mM sulfonic acid and the flow rate was 2 ml/min for both anions and cations. The detection limits for the different species were: $Cl^- = 0.03$ µmol, $K^+ = 0.03$ µmol and $CrO_4^{2-} = 0.01$ µmol $= 2 \times 10^{-9}$ mol/cm^2.

Scanning Electron Microscopy with Energy Dispersive X-ray Spectroscopy, SEM/EDX

The microscopy analysis was performed in an FEI Quanta 200 FEG ESEM operated in high vacuum mode. The instrument was equipped with an Oxford Inca EDX system, which was used for chemical quantification and elemental mapping. The ESEM was operated at 8–10 kV for imaging, and at 8–12 kV for EDX analysis. A Leo ULTRA 55 FEG SEM was also used together with an in-lens detector for imaging at high magnification.

Auger Electron Spectroscopy, AES

Auger electron spectroscopy was used to estimate oxide scale thickness and to determine elemental depth distribution. The AES analyses were performed with a PHI 660 scanning auger microprobe (SAM) using an accelerating voltage of 10 kV and a beam current of nA. AES depth profiling was performed using ion sputtering with 3.5 keV Ar^+. Two areas were analysed; one smaller 10×10 µm^2 and one larger 90×120 µm^2. They exhibited almost the same oxide thickness and elemental depth distribution. Only results from the small areas are shown in this study.

Quantitative analyses were performed using the peak-to-peak height of the Auger transitions of a specific element together with sensitivity factors provided by PHI, except for the Al and O, which were calibrated against pure Al_2O_3. Since the sensitivity factor for oxygen in Cr_2O_3 and Fe_2O_3 are different from that for Al_2O_3, the oxygen signal will be slightly off when mixtures of the oxides are present [19]. The computer software PHI-Matlab and linear least square (LLS) routines were used to separate the oxide and metal components in the depth profiles. This ensures that the detected Fe, Cr and Al in the oxide part of the depth profiles really are in oxidized form and consequently do not originate from the metal substrate.

Time of Flight-Secondary Ion Mass Spectrometry, ToF-SIMS

Time of flight-secondary ion mass spectrometry analyses were performed with a PHI TRIFT II instrument using a pulsed liquid metal ion gun (LMIG) enriched with $^{69}Ga^+$ ions. Depth profiles were obtained by sputtering a surface area of 50×50 µm^2 with a continuous non-pulsed beam with primary ion energy of 15 kV and a current of 20 nA. Positive and negative static SIMS modes were used to analyse an area of 25×25 µm^2 in the centre of the sputtered area. All SIMS spectra were calibrated using the exact positions of peaks with a known mass/charge ratio, such as aluminium ($^{26}Al^+$), chromium ($^{52}Cr^+$), iron ($^{56}Fe^+$) and the Ga primary ion ($^{69}Ga^+$). The intensities are expressed as peak areas rather than peak

heights, because the energy distribution is not the same for all secondary ions. Before imaging the sample surfaces, the optimum sputtering time for removing surface contamination while at the same time saving the remnants of previous surface deposit was 6 min using 2 nA, 25 kV $^{69}Ga^+$ rastered over a $200 \times 200 \text{ } \mu m^2$ area. The images were acquired during a sampling time of 8 min in both positive and negative modes.

Results

The Effect of Water Vapour on Oxidation

Gravimetry

Oxidation of Kanthal® APMT at 600 °C in the absence of KCl resulted in very low mass gains in both O_2 and $O_2 + H_2O$ environments (Figs. 2, 3). The in situ TG measurements (Fig. 3) indicate that mass gain is somewhat greater in the presence of water vapour. The higher noise in the TG measurement in $O_2 + H_2O$ (Fig. 3) is due to the presence of the humidifier. After completion of the TG exposures (168 h) the mass gains were 3.4 $\mu g/cm^2$ in O_2 and 6.1 $\mu g/cm^2$ in $O_2 + H_2O$, as determined ex situ.

XRD

After 24 h exposure in dry O_2 and in $O_2 + H_2O$ environments, rhombohedral M_2O_3 was identified, corresponding to Cr_2O_3, α-Fe_2O_3 or a solid solution of the two (Fig. 4). The analysis showed that the peak positions correspond to Cr_2O_3 and not α-Fe_2O_3. However, the peak positions are also compatible with Cr-rich $(FeCr)_2O_3$, especially in the dry O_2 environment. There was no indication of crystalline aluminium oxides and little evidence of spinel oxides. After 168 h, the rhombohedral M_2O_3 peaks became more pronounced, and the peak positions corresponded to pure Cr_2O_3 (Fig. 5). In addition, a weak peak appeared corresponding to spinel oxide (M_3O_4) with a unit cell slightly smaller than that of magnetite. It is suggested that this phase corresponds to FeCr- or FeCrAl-spinel oxide. Similar to the 24-h exposure there was no indication of crystalline aluminas.

AES

Figure 6 shows depth profiles acquired using AES after exposure to O_2 and $O_2 + H_2O$ at 600 °C for 24 and 168 h. In all cases, the oxide film was dominated by aluminium with significant amounts of iron and chromium present. Chromium was enriched in a band in the middle of the oxide film and iron oxide was consistently found outside the chromia band. The AES profiling showed that the oxide formed in dry O_2 was somewhat thinner than in $O_2 + H_2O$, i.e. the oxide was 19 nm in the dry environment and 24 nm in the wet environment after 24 h. After 168 h the film thickness had grown to 29 nm in dry and 36 nm in wet environment. This is in general agreement with the mass gains recorded (ex situ) in the TG exposures,
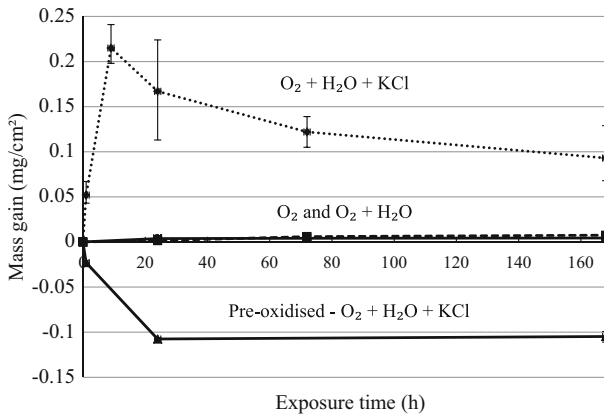
Fig. 2 Mass gain versus exposure time for untreated and pre-oxidised Kanthal® APMT. The samples were exposed at 600 °C in 5 % O_2 + 40 % H_2O in the presence of 0.1 mg/cm² KCl. The corresponding mass gain cuves for KCl-free samples are shown as reference (see also Fig. 3)
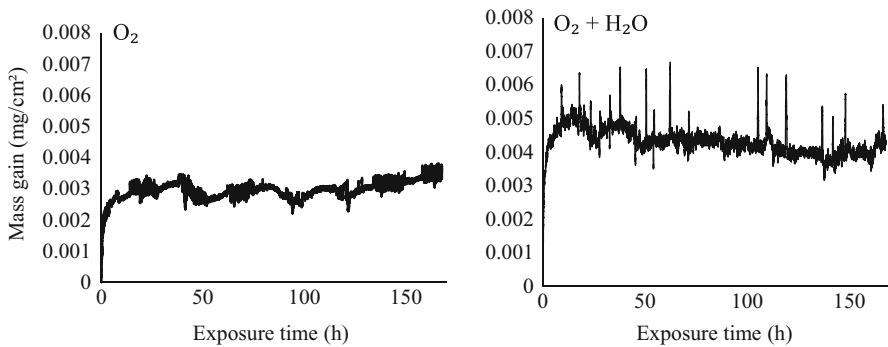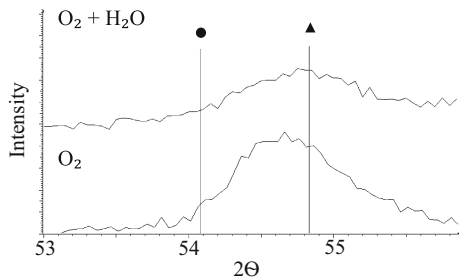

Fig. 3 TGA curves (In-situ mass gain versus exposure time) for Kanthal® APMT at 600 °C in 5 % O_2 and 5 % O_2 + 40 % H_2O

Fig. 4 XRD diffractograms of Kanthal® APMT exposed at 600 °C in 5 % O_2 and 5 % O_2 + 40 % H_2O for 24 h. The *symbols* indicate the peak positions of Cr_2O_3 (*Black filled triangle*) and α-Fe_2O_3 (*Black filled circle*) (h,k,l)

corresponding to an average thickness of the external oxide of 20 nm in the dry environment and 36 nm in the wet environment after 168 h. The chromia band formed early during exposure and appeared not to change with time (see

Fig. 5 XRD diffractograms of Kanthal® APMT exposed at 600 °C in 5 % O_2 and 5 % O_2 + 40 % H_2O for 168 h. The *symbols* indicate: Cr_2O_3 (*Black filled triangle*), M_3O_4 (*Black filled diamond*) and substrate (*Black filled square*)
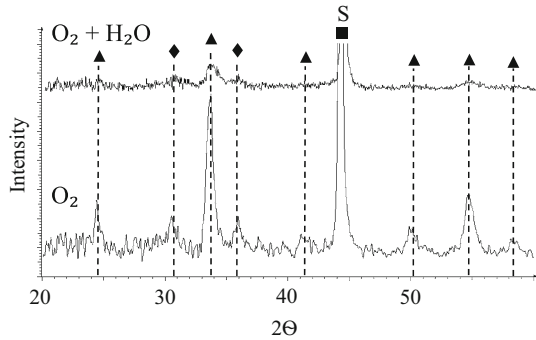
"Discussion" section). If the chromia band is considered to be a marker for the original sample surface, the additional oxide formed between 24 and 168 h is mainly due to inward growth. The alumina content in the outer part of the scale increased with exposure time.

SEM/EDX

In both environments, 168 h of oxidation resulted in a sample surface that was smooth and rather featureless. High magnification SEM showed 100 nm plate-like crystallites with sharp edges (Fig. 7a) in the dry environment, while in the presence of water vapour the oxide surface was dominated by <50 nm equiaxed grains (Fig. 7b), and the surface was corrugated.

Oxidation in the Presence of KCl

Gravimetry

Adding KCl to the polished samples before exposure to O_2 + H_2O at 600 °C resulted in much larger mass gains (Fig. 2). The mass gain increased rapidly up to 9 h and then decreased with exposure time. As no spallation was observed, the mass loss implies volatilization from the samples.

XRD

Figure 8 shows XRD patterns acquired after 24 and 168 h of exposure. KCl was only detected after 1 h (not shown). Potassium chromate (K_2CrO_4) was detected in all cases except after 168 h. A rhombohedral corundum-type solid solution $(FeCr)_2O_3$ formed initially on the surface (not shown). The corresponding peak positions shifted slightly toward a lower angle with exposure time, indicating an increase in cell volume attributable to an increase in iron content. After 168 h the positions of the main peaks corresponded to hematite (α-Fe_2O_3), representing the iron-rich end point of the solid solution $(FeCr)_2O_3$. In addition, weak peaks were detected after 24 and 168 h, indicating the presence of Cr_2O_3 (see Fig. 8).
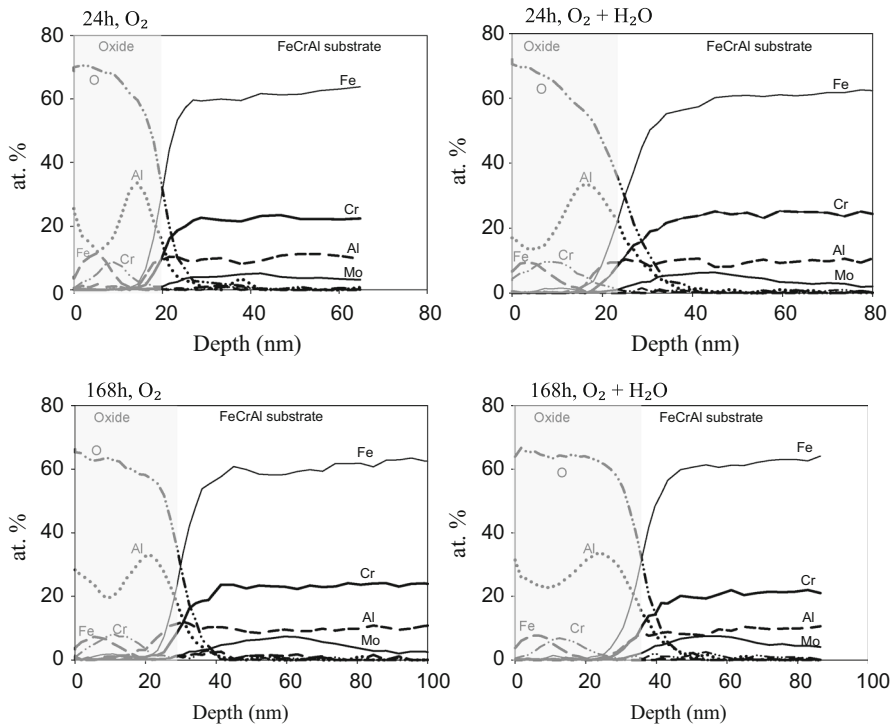
Fig. 6 AES depth profiles of samples exposed at 600 °C in 5 % O_2 and 5 % O_2 + 40 % H_2O for 24 and 168 h
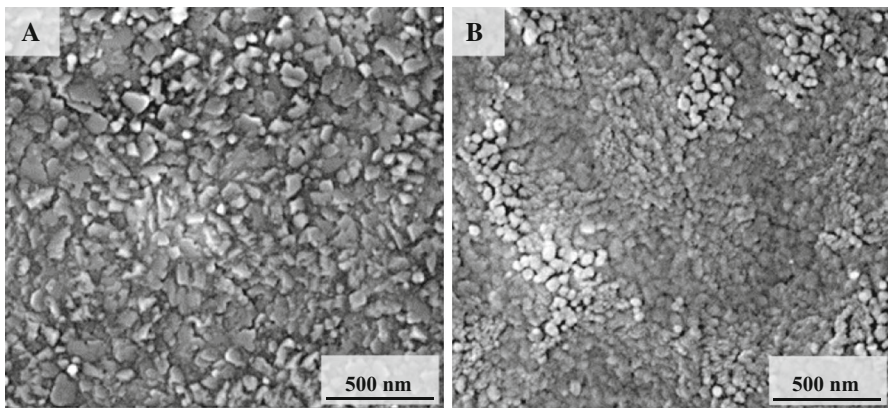

Fig. 7 In-lens SE images of Kanthal® APMT exposed at 600 °C for 168 h in 5 % O_2 (a) and 5 % O_2 + 40 % H_2O (b)
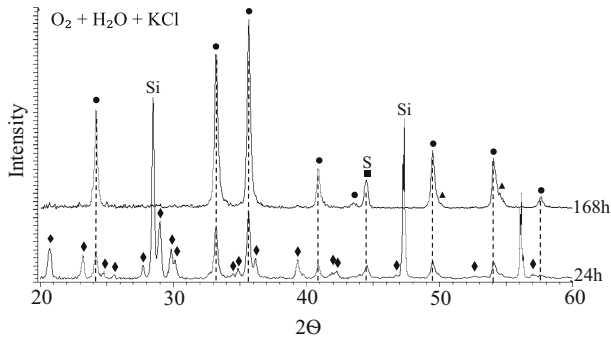
Fig. 8 X-ray diffractograms of Kanthal® APMT exposed at 600 °C in 5 % O_2 + 40 % H_2O in the presence of KCl for 24 and 168 h. The *symbols* indicate: K_2CrO_4 (*Black filled diamond*), α-Fe_2O_3 (*Black filled circle*), Cr_2O_3 (*Black filled triangle*), and substrate (*Black filled square*)

IC

Figure 9 shows the amount of water-soluble anions and cations extracted from the samples after exposure in the presence of KCl. While the amounts of K^+ and Cl^- both decreased with exposure time, chloride was lost more rapidly. Thus, after 1 h, only 57 % of the added chloride was retrieved from the samples, while almost all of the potassium (96 %) was detected. After 9 h only a small fraction of the added chloride remained on the surface. The analysis showed that substantial amounts of chromate (CrO_4^{2-}) formed on the steel surface. The stoichiometric relationship between K^+, Cl^- and CrO_4^{2-} on the sample surface after 1, 9 and 24 h (see Table 2) indicates that KCl reacts with chromia in the oxide scale according to:

$$1/2Cr_2O_3(s) + 2KCl(s) + 3/4O_2(g) + H_2O(g) \rightarrow K_2CrO_4(s) + 2HCl(g) \qquad (1)$$
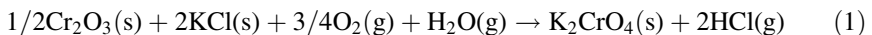
The amount of CrO_4^{2-} peaked at 9 h. Since scale spallation was not observed, the decrease in CrO_4^{2-} after >9 h implies that the chromate has decomposed. The deviations from the stoichiometry of Reaction (1) found after 72 and 168 h are attributed to the small amounts of K^+, Cl^- and CrO_4^{2-} that remained on the surface, resulting in relatively large measurement errors.

SEM/EDX

The SEM images of an unexposed sample in Fig. 10 show 10–100 μm KCl crystallites on the surface. The back scattered image (Fig. 10a) shows no signs of KCl between the salt particles. However, Fig. 10b, which was acquired with an in-lens SE detector, clearly shows small bright KCl particles between the large crystals. The presence of small amounts of KCl between the large crystals was verified using EDX.

The presence of KCl on the surface caused rapid corrosion and a surface morphology that changed with exposure time. The morphology can be described in terms of a few features: (i) partly reacted salt crystals with corrosion products; (ii) corrosion product agglomerations formed at completely reacted salt crystals; (iii)
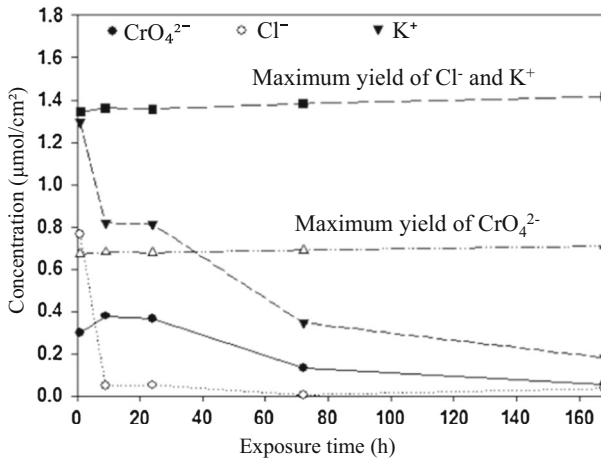
Fig. 9 Amount of water-soluble ionic substances on the sample surface versus exposure time for Kanthal® APMT exposed at 600 °C in 5 % O_2 + 40 % H_2O in the presence of KCl

Table 2 Quantitative analysis of water-soluble ions on the samples after exposure (μmol/cm^2)

Exposure time (h)	K^+	Cl^-	CrO_4^{2-}	$\frac{nk^+}{ncl^- + 2ncro_4^{2-}}$
1	1.29	0.76	0.30	0.95
9	0.82	0.05	0.38	1.01
24	0.81	0.05	0.37	1.03
72	0.35	0.00	0.13	1.30
168	0.18	0.04	0.05	1.29

The column to the right shows the stoichiometry of the reaction between KCl and Cr_2O_3. Reaction (1) corresponds to a ratio = 1
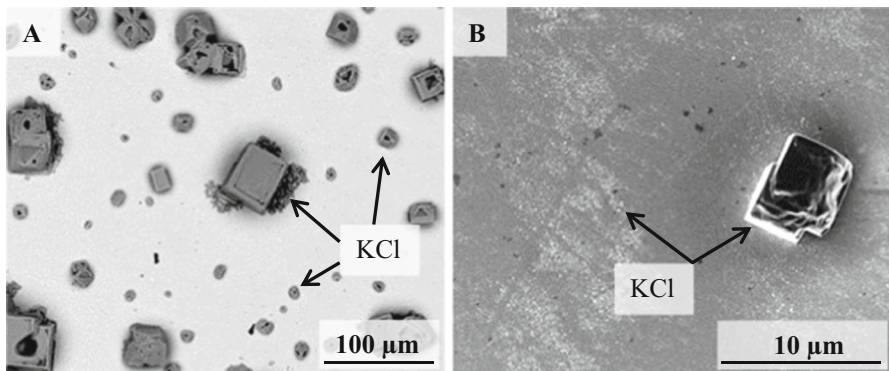

Fig. 10 SEM images of Kanthal® APMT with added KCl before exposure, (**a**) is a BSE and (**b**) an SE image taken with an in-lens detector

the oxide between (i) and (ii); and (iv) chromate particles on top of the oxide and on the former salt crystals. These morphological features will be described in more detail below.

1 h

SEM analyses after 1 h in 5 % O_2 + 40 % H_2O in the presence of KCl showed numerous small particles (1–3 μm) on the alloy surface (Fig. 11 a, b). Figure 12 shows EDX maps of a partly reacted/evaporated KCl crystal surrounded by small particles that sit on a relatively smooth oxide. The EDX maps show that the small particles mainly contain K, Cr and O, suggesting that they consist of K_2CrO_4, which was identified using XRD (compare Fig. 8). The presence of CrO_4^{2-} was also verified with IC (Fig. 9). As expected, some areas contained large amounts of Cl and K, corresponding to the KCl identified with XRD. The presence of substantial amounts of unreacted KCl at this stage is also in accordance with the IC analysis (Fig. 9). In addition to the large, partly reacted KCl crystals, small amounts of Cl and K were present in the smooth oxide between the K_2CrO_4 particles; the EDX analysis indicated about 1–2 at.% K and Cl. The surface coverage of K_2CrO_4 varied; in some areas the chromate particles formed a circle around the partly reacted KCl crystals (Fig. 11b), and in some areas the K_2CrO_4 particles agglomerated to form a layer that tends to be cracked (Fig. 11a). The cracks are suggested to be due to the relatively large thermal expansion coefficient of K_2CrO_4 (about 50 × 10^{-6}/K [20] compared to 13.6 × 10^{-6}/K for the alloy) that causes stresses during cooling. At this stage, some of the KCl crystals became more or less overgrown by the iron-rich oxide that formed shell-like aggregates, roughly replicating the shape of the original salt particles (Fig. 11b).

24 h

With time, the scale surface became increasingly iron-rich and after 24 h of exposure most of it consisted of iron oxide. The iron oxide appears bright in Fig. 11c and d and is assumed to correspond to hematite, which was identified with XRD (see Fig. 8). KCl is absent from the surface at this stage; the former salt crystals were replaced by the oxide accumulations that often tend to form shell-like structures. Compared to the particles after 1 h, the K_2CrO_4 particles (dark grey in Fig. 11c, d) had grown in size after 24 h of exposure and showed a tendency to agglomerate in certain areas. K_2CrO_4 particles could be found on top of some oxide agglomerations (former KCl crystals), in some cases covering them entirely as shown in Fig. 11d. Some of the reacted salt crystals were surrounded by a circular halo of thin oxide. On top of the thin oxide there were morphological features with a distribution and shape similar to that of the K_2CrO_4 particles seen after 1 h (Fig. 13a, b). SEM/EDX showed traces of chromate in these features and they are assumed to correspond to partly decomposed K_2CrO_4. EDX point analyses showed no indication of Cl in the former salt particles and overgrown areas. Small amounts of chlorine (1–2 at.%) and slightly higher amounts of potassium were detected in areas not yet overgrown by iron oxide. In accordance with the EDX analysis, the IC results showed that only 4 % of the added chloride remained on the surface after 24 h of exposure (Table 2).
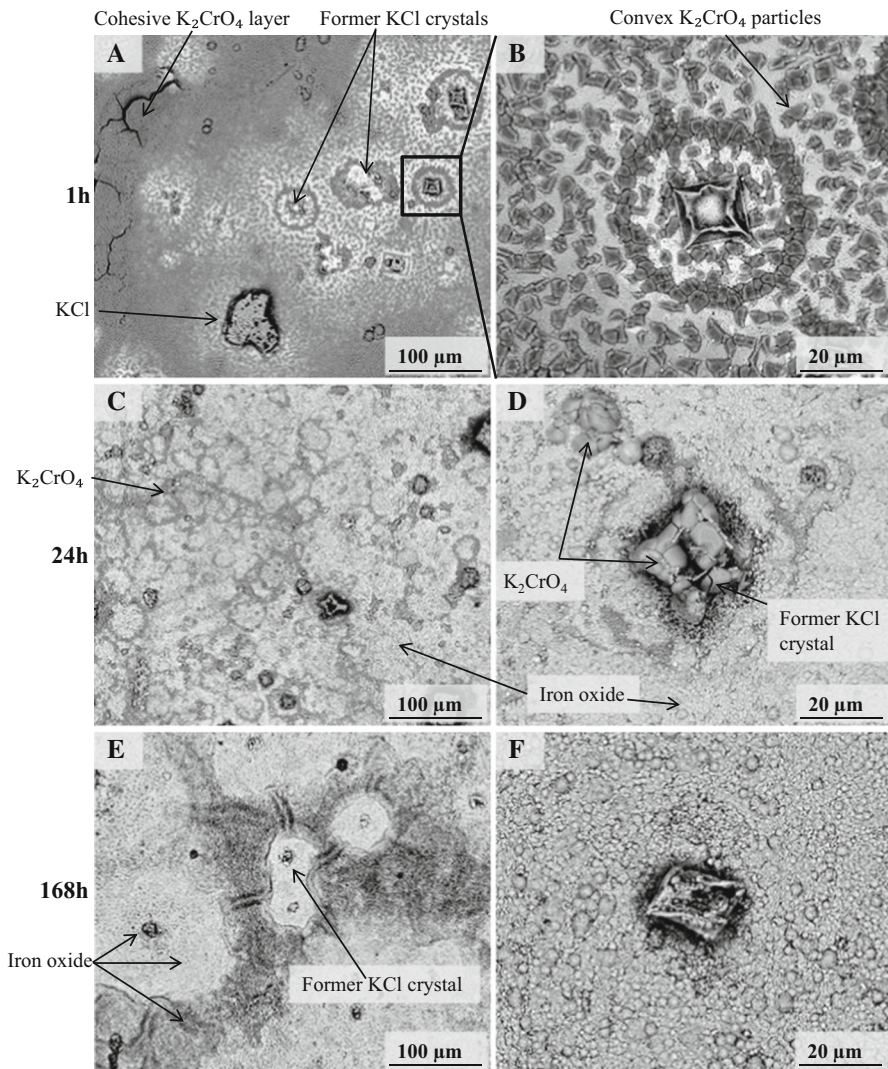
Fig. 11 SEM BSE images of Kanthal® APMT exposed at 600 °C for 1 h (**a**, **b**), 24 h (**c**, **d**) and 168 h (**e**, **f**) in 5 % O_2 + 40 % H_2O with KCl

168 h

After 168 h the entire surface was overgrown by iron-rich oxide, and ridges of iron-rich oxide surrounded the former salt crystals (Fig. 11e). EDX point analyses showed that the ridges contained slightly more potassium (~ 2 at.%) and chromium (~ 4 at.%) than the base oxide. The surface of the oxide ridges contained small rounded "pockmark" features, (see Fig. 14) corresponding to the partly decomposed K_2CrO_4 particles observed after 24 h (compare Fig. 13b). The oxide formed
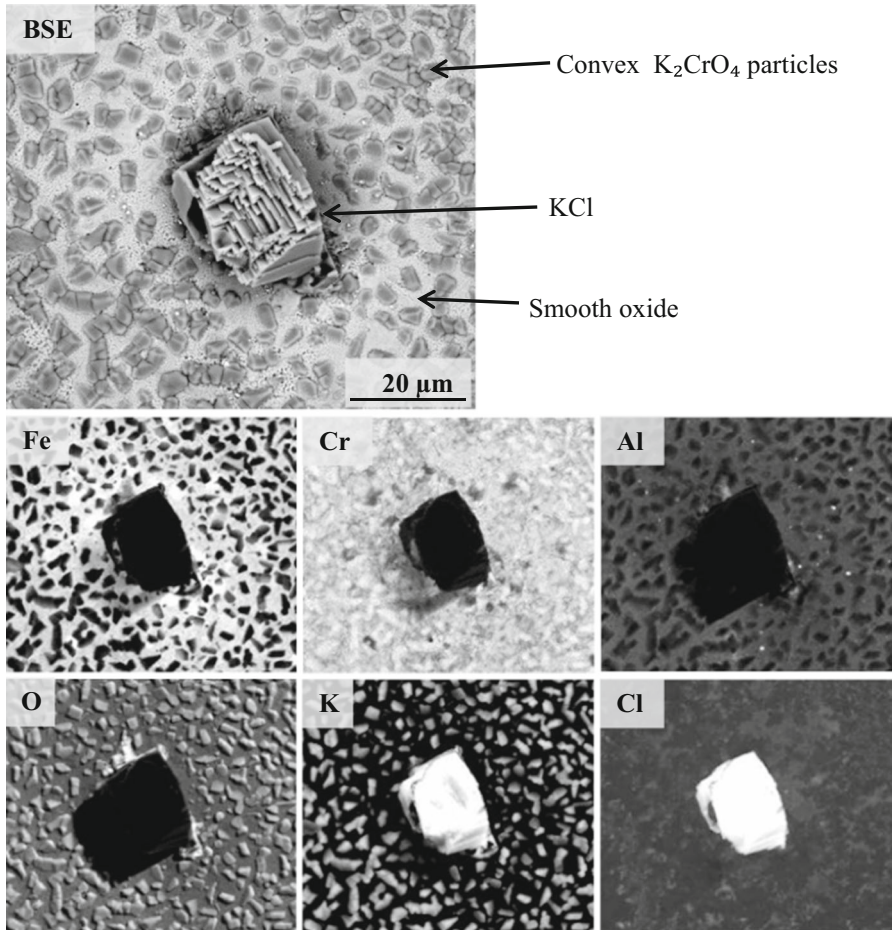
Fig. 12 SEM BSE image and EDX elemental maps of Kanthal[®] APMT exposed at 600 °C for 1 h in 5 % O_2 + 40 % H_2O with KCl

after 72 h (not shown) is similar to that observed after 168 h except that the amount of K_2CrO_4 is greater after 72 h.

Pre-oxidation at 700 °C in 20 % O_2 ± 80 % N_2

Pre-oxidation in the tube furnace for 24 h resulted in an average mass gain of 12 µg/ cm^2. The mass gain is in accordance with the Auger analysis, showing that the oxide film is about 70 nm thick, aluminium-rich and contains traces of chromium and iron, as shown in Fig. 15a. The oxide is similar to that formed in the exposures at 600 °C except that it is thicker and more Al-rich. The oxide morphology is smooth with a grain size ∼100 nm and similar to that formed after 168 h at 600 °C in the dry O_2 environment [21]. Similar to the 168-h exposure at 600 °C, the XRD
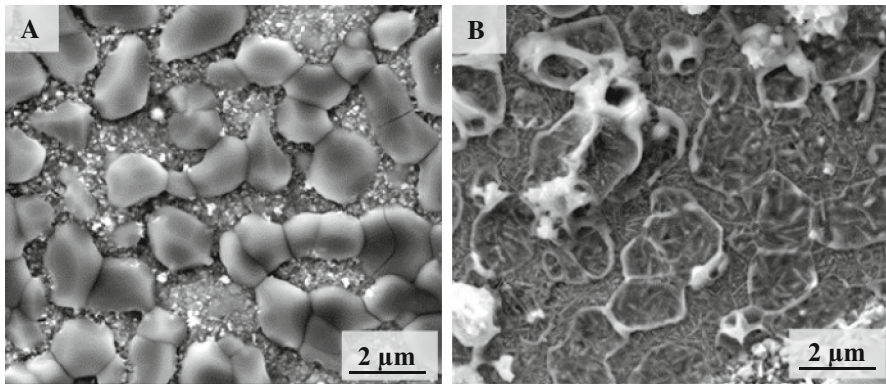
Fig. 13 SEM SE images of Kanthal® APMT exposed at 600 °C for 1 h (**a**) and 24 h (**b**) in 5 % O_2 + 40 % H_2O with KCl. Image (**a**) shows K_2CrO_4 particles on the surface and image (**b**) shows the remains of the K_2CrO_4 particles after 24 h of exposure
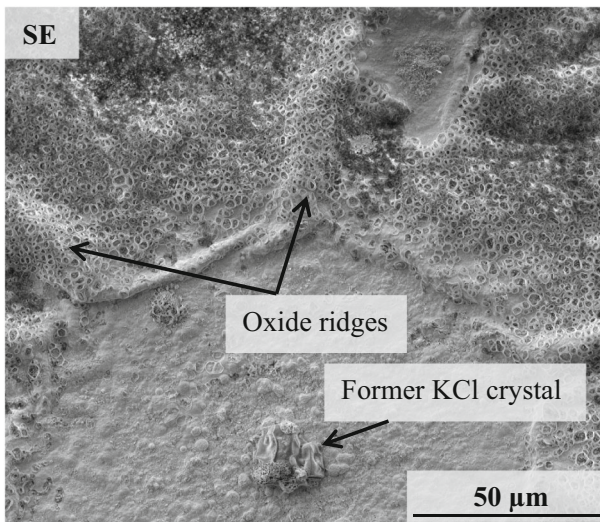

Fig. 14 SEM SE image of Kanthal® APMT exposed at 600° C for 168 h in 5 % O_2 + 40 % H_2O with KCl

spectrum gave evidence of the presence of Cr_2O_3 while no crystalline alumina phases could be positively identified (see Fig. 16).

The Effect of KCl, Oxygen and Water vapour on Pre-Oxidized Samples

Gravimetry

Exposing the pre-oxidized samples at 600 °C in the presence of KCl initially resulted in a mass loss. After 24 h no further change in mass was registered (Fig. 2). The measured mass loss closely corresponds to the amount of salt added before exposure (0.10 mg/cm^2) and is attributed to the volatilization of KCl.
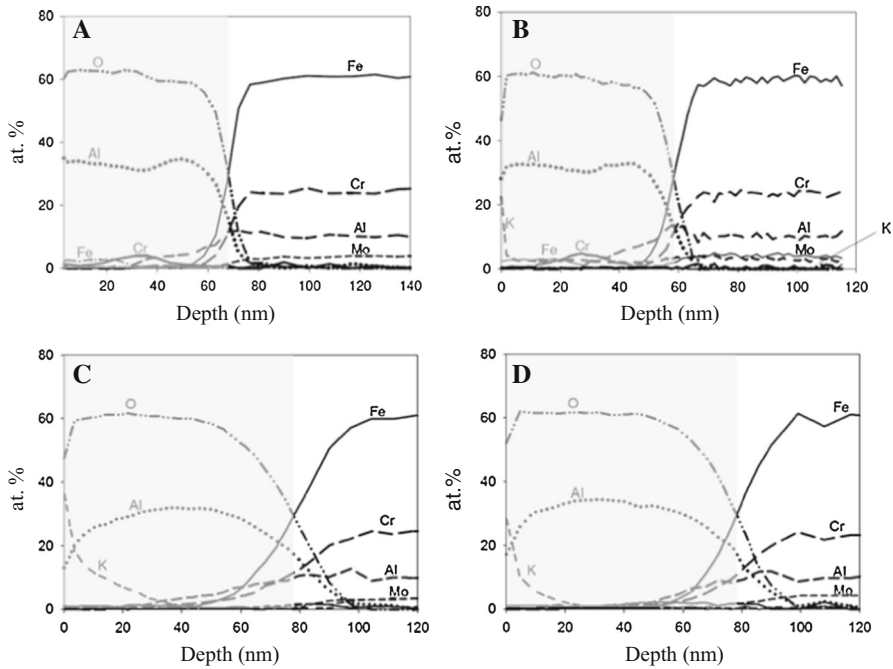
Fig. 15 AES depth profiles of pre-oxidised Kanthal® APMT at 700 °C for 24 h (**a**), pre-oxidised Kanthal® APMT with added KCl and exposed additionally for (**b**) 1, (**c**) 24 and (**d**) 168 h at 600 °C
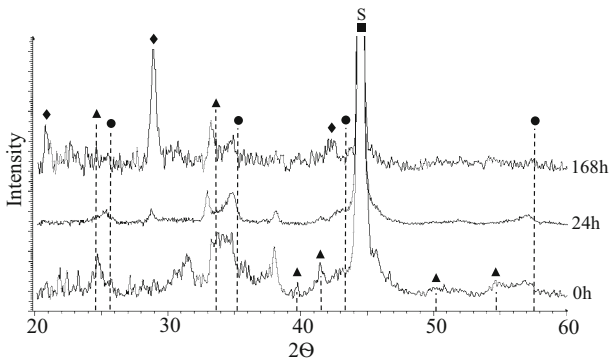

Fig. 16 X-ray diffractograms of pre-oxidised Kanthal® APMT at 700 °C for 24 h and subsequently exposed at 600 °C in 5 % O_2 + 40 % H_2O in the presence of KCl for 24 and 168 h. The *symbols* indicate: Cr_2O_3 (*Black filled triangle*), α-Al_2O_3 (*Black filled circle*), $KAlSiO_4$ (*Black filled diamond*) and substrate (*Black filled square*)

XRD

After 1 h, there were no additional diffraction peaks except for KCl (not shown). KCl was not detected after longer exposure times. The XRD analysis performed after 24 h exposure showed diffraction lines that are tentatively attributed to α-

alumina (Fig. 16). After 24 h and especially after 168 h, a new set of diffraction lines appears that are tentatively attributed to $KAlSiO_4$ (Kaliophilite) (see Fig. 16). The Cr_2O_3 observed directly after pre-oxidation and after 1 h of exposure with KCl, was absent after 24 and 168 h.

IC

Figure 17 and Table 3 show the amount of water-soluble anions and cations found on the pre-oxidized samples after exposure with KCl. After 1 h, 78 % of the added Cl and 89 % of the K were found, while no CrO_4^{2-} was detected. The mismatch between the Cl^- and K^+ concentrations and the absence of CrO_4^{2-} implies that K must be present in a form other than KCl or K_2CrO_4. The potassium and chloride concentrations decreased with time in a similar manner and the concentrations remained constant after 24 h. Only traces of chromate (CrO_4^{2-}) were recorded (corresponding to <0.5 % of the added K).

SEM/EDX

1 h   One hour of exposure in the presence of KCl produced little change in surface morphology (compare Figs. 10a, 18a).This is in marked contrast to the material not subjected to pre-oxidation (compare Fig. 11a). However, a few K_2CrO_4 particles were detected on the surface with EDX (Fig. 18b). In line with the slow corrosion attack, the KCl crystals were less reacted than the crystals in the exposure without pre-oxidation (see Figs. 11, 12).

24 h   There was no indication of KCl on the surface after 24 h (Fig. 18c, d), and the KCl crystals left no morphological traces on the surface. The number of K_2CrO_4 particles was greater than in the 1 h exposure, appearing as dark spots in Fig. 18c. In comparison to the corresponding exposure without pre-oxidation, the amount of K_2CrO_4 was much less, in accordance with the IC analysis (Table 3). Based on the number density and size of the K_2CrO_4 particles, the amount of chromate on the surface was estimated to be about 1×10^{-8} mol/cm^2. As noted above, the oxide scale formed during pre-oxidation contained a chromium-rich band. Integrating the Cr signal in the Auger profile in Fig. 15a indicates that the amount of Cr in the scale corresponds to a 1–1.5 nm thick layer of pure Cr_2O_3, corresponding to $8–12 \times 10^{-9}$ mol/cm^2 of Cr. The agreement regarding the amount of Cr implies that the chromium in the pre-oxidation scale is the only source of chromate on the surface. This conclusion is supported by the AES profiling (see below). Typically, K_2CrO_4 particles were considerably larger than without pre-oxidation. However, small K_2CrO_4 particles were also observed. At this stage porous oxide agglomerate of different sizes appeared on the surface that was enriched in K and Si and also contained Al, together with some Cr and Fe (see Fig. 18d). In addition to the larger porous agglomerates seen in Fig. 18d, smaller ones (0.5–1 μm) were scattered over the surface (not shown). Iron-rich oxide had started to grow in the vicinity of some of the K_2CrO_4 particles (Fig. 19). Otherwise there were no signs of corrosion.
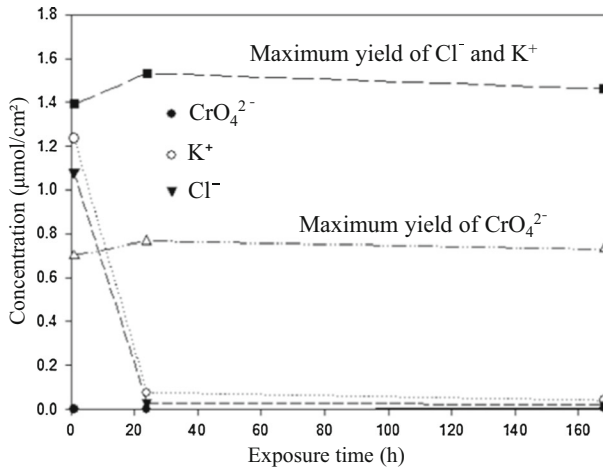
Fig. 17 Amount of water-soluble ionic substances on the sample surface versus exposure time for pre-oxidised Kanthal® APMT with added KCl exposed at 600 °C in 5 % O_2 + 40 % H_2O for 1, 24 and 168 h

Table 3 Water-soluble ions after exposure of pre-oxidised samples with KCl ($\mu mol/cm^2$) and stoichiometry of Reaction (1)

Exposure time (h)	K^+	Cl^-	CrO_4^{2-}	$\frac{n_{k^+}}{n_{cl^-}+2n_{cro_4^{2-}}}$
1	1.24	1.08	0	1.15
24	0.08	0.03	0	2.67
168	0.04	0	0	–

168 h The surface morphology after 168 h was similar to that described after 24 h, showing little evidence of a corrosion attack. At this stage the K_2CrO_4 particles had been replaced with porous agglomerates of similar size and distribution. It is proposed that these agglomerates are the remnants of decomposed K_2CrO_4 particles. Based on EDX point analyses, the porous agglomerates (see Fig. 18f) are enriched in Si, K and O and also contain considerable amounts of Al.

AES AES depth profiling performed after 1 h exposure at 600 °C in the presence of KCl, showed little change compared to the pre-oxidised sample, except that K was present at the surface (Fig. 15b). The alumina scale continued to increase in thickness up to 24 h (to about 80 nm), however no further increase in thickness was detected after 168 h. The depth profiles acquired after 24 and 168 h of exposure with KCl (Fig. 15c, d) indicate that potassium is mainly situated in the outer 20 nm of the oxide. However, there are also traces of potassium deeper into the scale. It may be noted that the chromia-enriched band observed in Fig. 15a, b had disappeared after 24 and 168 h. Considering the simultaneous occurrence of K_2CrO_4 on the scale surface (see Fig. 18b, c), it is proposed that most of the chromia in the scale had reacted with KCl according to Reaction (1). Iron in the
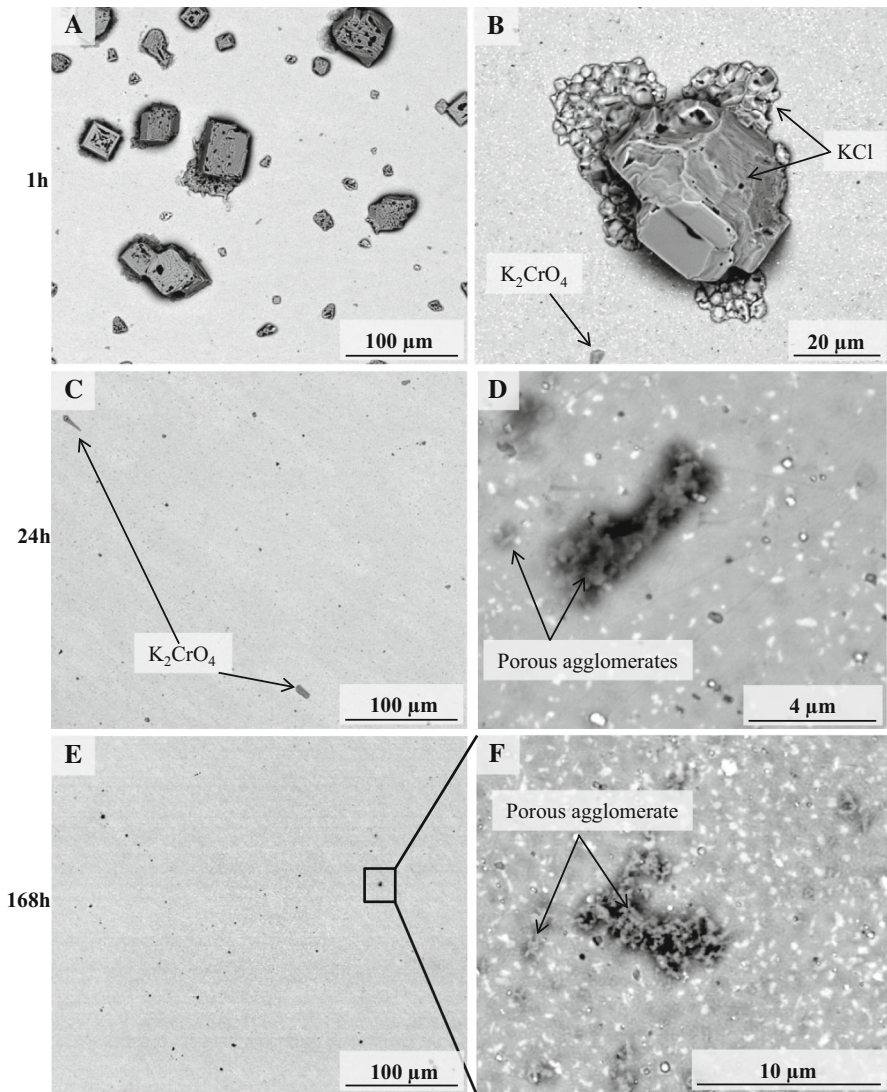
Fig. 18 SEM BSE images of pre-oxidised Kanthal® APMT exposed at 600 °C with KCl for 1 h (**a, b**), 24 h (**c, d**) and 168 h (**e, f**) in 5 % O_2 + 40 % H_2O

scale behaved similar to chromium and had a tendency to disappear with time. However, we did not observe iron-containing corrosion products on the surface in sufficient quantity to account for the missing iron oxide within the scale. Mo was present in the alloy substrate and its distribution did not change upon exposure. Chlorine is not shown in the depth profiles because of the overlap of Auger electron energies with Mo in the alloy.
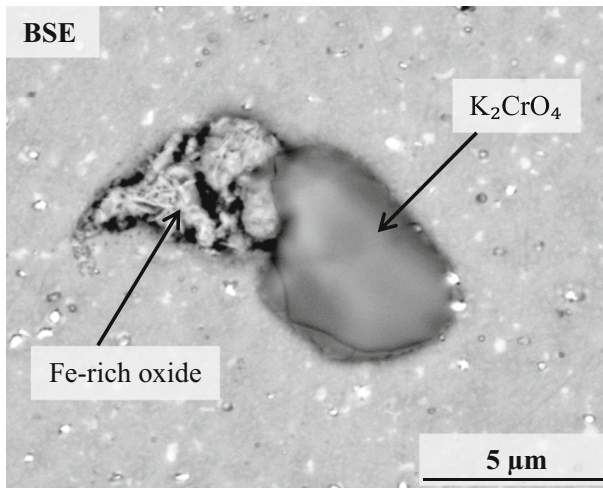
Fig. 19 SEM BSE images of pre-oxidised Kanthal$^{\circledR}$ APMT exposed at 600 °C with KCl for 24 h

Tof-SIMS Because of the difficulty of analysing Cl in the presence of Mo, a complementary analysis with SIMS was carried out. It may be noted that while the SIMS analysis has very high sensitivity (better than AES), it is not quantitative. Nevertheless, SIMS is still useful for comparing the concentration and distribution of a certain element in a scale, as a function of exposure time for example.

Figure 20 shows depth profiles for positive and negative ions from a pre-oxidised sample and from samples oxidised 24 and 168 h in the presence of KCl. The AlO_2^- ion signal in Fig. 20 is used here to indicate the interface between aluminium oxide and the metal substrate. The SIMS depth profiles for pre-oxidised Kanthal$^{\circledR}$ APMT (Fig. 20a) are in general agreement with the AES depth profile of the same material (Fig. 15a), showing an Al-rich oxide containing both chromium and iron. The analysis further indicates that silicon has been enriched at the scale surface. The traces of K and Cl found at the surface after pre-oxidation are due to contamination. After 24 and 168 h oxidation of the pre-oxidised material in the presence of KCl, the main change indicated by SIMS is an enrichment of K in the outer part of the oxide, in agreement with the AES results (Fig. 15). There was a decrease in the chromium and iron SIMS signals which is also in agreement with the AES analysis. Importantly, there was no indication that the chlorine penetrates the oxide and accumulates at the oxide/metal interface.

SIMS depth profiling was not performed on the sample oxidized with KCl for 1 h. However, imaging with SIMS (see [21]) showed a dendritic network of potassium and chlorine, which corresponds to the distribution of the added salt, and is similar to that observed with SEM on the unexposed material with added KCl (Fig. 10b).

Discussion

Oxidation of the powder-metallurgical FeCrAl alloy Kanthal® APMT at 600 and 700 °C in the absence of KCl, results in the formation of a thin oxide layer which is dominated by alumina and contains significant amounts of iron and chromium. Similar results have been reported for conventional FeCrAl alloys with similar compositions at 500–900 °C in O_2 and $O_2 + H_2O$ [15, 16, 22]. It is notable that, although the oxide film is dominated by aluminium oxide (see Figs. 6, 15), no crystalline aluminas can be detected with XRD. This is also in accordance with Josefsson et al. [15] and Canovic et al. [22], who reported that FeCrAl oxidation produces no crystalline aluminas at 500 and 600 °C. However, Josefsson et al. [15] detected α-Al_2O_3 after 168 h at 700 °C. It is well-known that FeCrAl alloys tend to form metastable aluminium oxides at "low temperatures", see e.g. Stott, Wood and Stringer [23]. The present results imply that the alumina in the oxide film is metastable and amorphous/poorly crystalline.

The observation that rhombohedral Cr-rich $(FeCr)_2O_3$ forms initially and becomes increasingly Cr-rich with time is also in agreement with Josefsson et al. [15]. In accordanc with Liu et al. [24] (working at 900 °C), it is proposed that the iron and chromium in the alumina film enters the film during transient oxidation, i.e., during and immediately after heat-up of the sample. The observation that the oxide film grows both inward and outward (see Fig. 6) agrees with reports on FeCrAl oxidation at 800 and 900 °C by Li et al. and Czyrska-Filemonowicz et al. [25, 26]. Although the rates are very small, the results show that oxidation is somewhat faster in an $O_2 + H_2O$ environment than in dry O_2. Oxidation of the FeCrAl alloy Kanthal® AF at 900 °C in O_2 and $O_2 + H_2O$ environment by Li et al. and Götlind et al. showed that the acceleration of oxidation by water vapour is attributed to the kinetic stabilization of relatively fast-growing metastable aluminas relative to the more slow growing α-alumina [25, 27]. However, in the present study there is no indication that the phase composition of the protective film is influenced by water vapour. In general the XRD intensities are higher in the O_2 than in $O_2 + H_2O$ environment, while the mass gains are consistently lower in the former. This suggests that the oxide film formed in dry O_2 is more crystalline. No signs of chromium volatilization were detected on the FeCrAl alloy APMT in the presence of water vapour, as has been reported for stainless steels by Asteman et al. [11].

The results clearly illustrate that KCl is strongly corrosive towards the as-polished alloy in an $O_2 + H_2O$ environment at 600 °C. The evidence from XRD and SEM/EDX (formation of K_2CrO_4, consumption of KCl) and the quantitative IC analysis $\left(n_K^+ - n_{Cl}^- = 2nCrO_4^{2-}\right)$ (see Figs. 8, 9, 11; Table 2) shows that Cr_2O_3 on the surface reacts with KCl to form potassium chromate according to Reaction (1) (see above). Similar observations have been reported for a conventional FeCrAl alloy using the same experimental conditions [28]. In that case it was argued that breakaway oxidation in an $O_2 + H_2O$ environment is triggered by chromate formation. Thus, in an $O_2 + H_2O + KCl$ environment, chromate formation through reaction (1) depletes the protective scale in Cr, triggering the formation of a fast-growing iron-rich oxide scale. Chromate formation has been observed from 400 °C
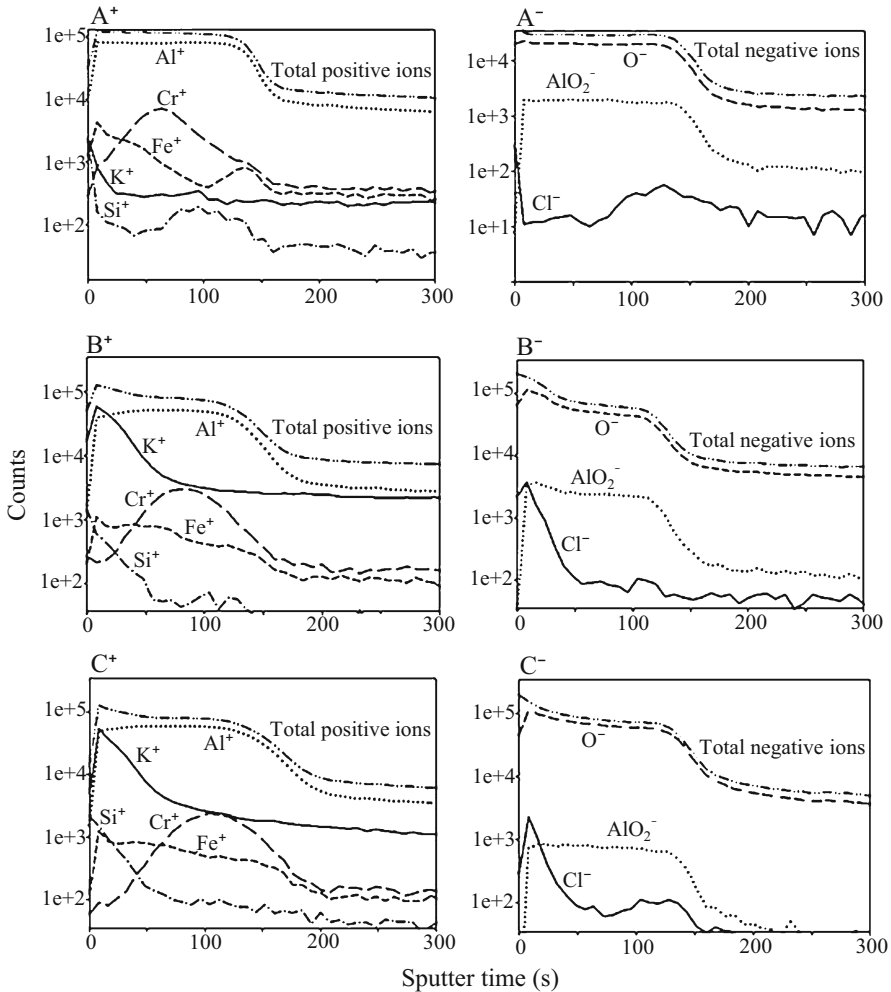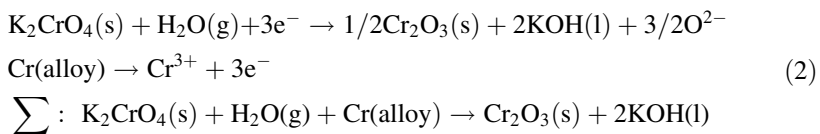
Fig. 20 ToF-SIMS sputter depth profiles in the oxide scales formed on Kanthal® APMT samples after pre-oxidation for 24 h at 700 °C in 20 % O_2 (**a**), pre-oxidised Kanthal® APMT with added KCl and exposed additionally for 24 and 168 h at 600 °C in 5 % O_2 + 40 % H_2O (**b**) and (**c**)

on stainless steel by Pettersson et al. [29]. Thus, it is suggested that, in the present case, chromate formation begins during the sample heat-up, at the start of the exposure. Recently it has been reported by Israelsson et al. [28] that alloy chlorination occurs simultaneous with potassium chromate formation, especially in a dry O_2 environment. The two processes compete because potassium chromate formation results in the loss of chlorine from the surface in the form of HCl(g). Thus, it is suggested that the slight evidence for metal chlorination in the present study is due to Reaction (1), i.e., chlorine rapidly escaping from the surface as HCl(g) in an O_2+ H_2O environment.

The IC analysis shows that 57 % of the added salt remains after 1 h assuming that the soluble chlorine detected corresponds to KCl. Since 96 % of the potassium was detected it is concluded that only a small fraction of the salt had vaporised from the surface at this stage. Similar amounts of chromate were detected on the surface after 1 h of exposure of Kanthal® AF under the same experimental conditions [28], even though twice as much KCl was present. This suggests that the rate of Reaction (1) is initially not limited by the amount of KCl. Table 2 shows that the stoichiometry of Reaction (1) is only satisfied up to 24 h of exposure. This is related to the apparent decomposition of K_2CrO_4 with time (Figs. 9, 13, 14). Similar observations have been reported in [28] where the decomposition of K_2CrO_4 is attributed to the reduction of chromate by electrons originating from the oxidation of the alloy substrate in an electrochemical process:

$$K_2CrO_4(s) + H_2O(g) + 3e^- \rightarrow 1/2Cr_2O_3(s) + 2KOH(l) + 3/2O^{2-}$$
$$Cr(alloy) \rightarrow Cr^{3+} + 3e^- \tag{2}$$
$$\sum: \ K_2CrO_4(s) + H_2O(g) + Cr(alloy) \rightarrow Cr_2O_3(s) + 2KOH(l)$$

In accordance with this hypothesis, large amounts of potassium but very little chromate are present on the surface after long exposure times (see Table 2).

Although results show that pre-oxidation has a strongly beneficial effect on the high-temperature corrosion of Kanthal® APMT in an $O_2 + H_2O + KCl$ environment (see Figs. 2, 15, 17, 18), the formation of K_2CrO_4 on the surface (Fig. 18b, c) shows that the "protective oxide" formed in the pre-oxidation is not completely inert to KCl. However, in contrast to the untreated samples exposed to $O_2 + H_2O + KCl$, the reaction does not trigger breakaway oxidation, and the chromium for the reaction that forms chromate only originates from the oxide layer. Specifically, the appearance of surface chromate on the pre-oxidised surface is accompanied by the loss of chromia from the oxide layer (see Figs. 15, 20). As chromium in the protective oxide layer is invariably found in a band in the middle of the layer (Fig. 15a), this also implies that the other reactants necessary for chromate formation (KCl, O_2, H_2O) are able to penetrate the outer part of the oxide layer. As shown with SEM/EDX, the pre-oxidised material also forms numerous small porous agglomerates containing K, Al, Si and O on top of the "protective oxide" (see Fig. 18d, f). It is proposed that the porous agglomerates correspond to the $KAlSiO_4$ detected with XRD. This suggests that KCl has reacted with alumina and with the silica which was detected at the scale/gas interface after pre-oxidation (Fig. 20), according to Reaction (3) [30]:

$$H_2O(g) + 2SiO_2(s) + 2KCl(s) + Al_2O_3(s) \rightarrow 2HCl(g) + 2KAlSiO_4(s) \tag{3}$$
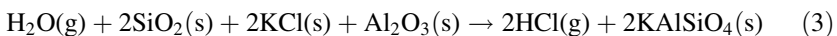
$\Delta G_{873K}^\circ = 53.756 \ \mathrm{kJmol^{-1}} \ K$ which gives P_{eq} HCl(g) = 0.015 atm (in 40 % H_2O).

The results show that the K_2CrO_4 particles tend to decompose with time. Thus, the large porous agglomerates in Fig. 18d, f are assumed to originate from the K_2CrO_4 particles observed after 24 h (Fig. 18c). The large agglomerates have a composition similar to that of the small porous agglomerates mentioned above.

Because the oxide formed in the pre-oxidation is relatively inert and slow-growing it is not considered likely that the decomposition of K_2CrO_4 on the pre-oxidised samples is mainly due to Reaction (2). Instead the following reaction is considered [30]:

$$2SiO_2(s) + K_2CrO_4(s) + Al_2O_3(s) \rightarrow 1/2Cr_2O_3(s) + 2KAlSiO_4(s) + 3/4O_2(g)$$
(4)
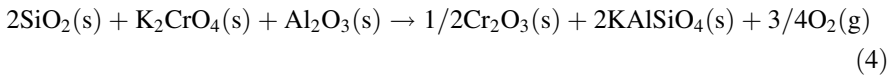
$$\Delta G^{\circ}_{873K} = -36.719 \, kJmol^{-1} \, K$$

According to Reaction (4), the large porous agglomerates are expected to contain chromia. It was not possible to determine whether or not this is the case with SEM/EDX because of the chromium signal from the underlying oxide and from the substrate. Alternatively, the following reaction would leave no chromia in the product [30]:

$$2H_2O(g) + 2K_2CrO_4(s) + 2Al_2O_3(s) + 4SiO_2(s) \rightarrow 2H_2CrO_4(g) + 4KAlSiO_4(s)$$
(5)
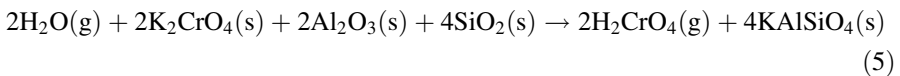
$\Delta G^{\circ}_{873K} = 88.760 \, kJmol^{-1} \, K$ which gives $P_{eq} \, H_2CrO_4 \, (g) = 884 \times 10^{-6}$ atm (in 40 % H_2O) However, further investigations are needed in order to establish if Reaction (4) or (5) is the dominant reaction, e.g. through measurement of $H_2CrO_4(g)$ in the gas flow after the furnace.

Conclusions

- KCl strongly accelerates the corrosion of Kanthal® APMT in $O_2 + H_2O$ at 600 °C. Chromia in the scale reacts rapidly with $O_2 + H_2O$ forming K_2CrO_4 and gaseous HCl. Chromate formation depletes the protective scale in Cr, triggering the formation of a fast-growing iron-rich scale.
- K_2CrO_4 is reduced on the scale surface according to an electrochemical process where the electrons are supplied by means of alloy oxidation.
- There was little evidence for alloy chlorination and it was believed to be of secondary importance in the present case.
- Pre-oxidation has a strong beneficial effect on the corrosion behaviour of the FeCrAl alloy in the presence of KCl at 600 °C.
- The oxide scale from the pre-oxidation at 700 °C is not completely inert to KCl since K_2CrO_4 forms on the surface.
- $KAlSiO_4$ forms on the pre-oxidised samples exposed to $O_2 + H_2O + KCl$.
- $KAlSiO_4$ is believed to form either by a reaction between KCl, H_2O and the oxide scale or by a reaction between K_2CrO_4, H_2O and the oxide scale.

References

1. H. P. Michelsen, F. Frandsen, K. Dam-Johansen and O. H. Larsen, *Fuel Processing Technology* **54**, 1998 (95).
2. B. Sander, *Biomass and Bioenergy* **12**, 1997 (177).
3. L. L. Baxter, T. R. Miles, T. R. Miles Jr, B. M. Jenkins, T. Milne, D. Dayton, R. W. Bryers and L. L. Oden, *Fuel Processing Technology* **54**, 1998 (47).
4. R. L. Bain, R. P. Overend and K. R. Craig, *Fuel Processing Technology* **54**, 1998 (1).
5. B. M. Jenkins, L. L. Baxter, T. R. Miles Jr and T. R. Miles, *Fuel Processing Technology* **54**, 1998 (17).
6. H. Kassman, J. Pettersson, B.-M. Steenari and L.-E. Åmand, *Fuel Processing Technology* **105**, 2013 (170).
7. P. Viklund, A. Hjörnhede, P. Henderson, A. Stålenheim and R. Pettersson, *Fuel Processing Technology* **105**, 2013 (106).
8. M. Montgomery and A. Karlsson, *Materials and Corrosion* **50**, 1999 (579).
9. R. A. Antunes and M. C. L. de Oliveira, *Corrosion Science* **76**, 2013 (6).
10. H. P. Nielsen, F. J. Frandsen, K. Dam-Johansen and L. L. Baxter, *Progress in Energy and Combustion Science* **26**, 2000 (283).
11. H. Asteman, J. E. Svensson and L. G. Johansson, *Oxidation of metals* **57**, 2002 (193).
12. C. Pettersson, L.-G. Johansson and J.-E. Svensson, *Oxidation of metals* **70**, 2008 (241).
13. S. Enestam, D. Bankiewicz, J. Tuiremo, K. Mäkelä and M. Hupa, *Fuel* **104**, 2013 (294).
14. P. Kofstad, *High Temperature Corrosion*, (Elsevier Applied Science Publishers Ltd, London, 1988).
15. H. Josefsson, F. Liu, J.-E. Svensson, M. Halvarsson and L.-G. Johansson, *Materials and Corrosion* **56**, 2005 (801).
16. H. Asteman and M. Spiegel, *Corrosion Science* **50**, 2008 (1734).
17. Y. S. Li, Y. Niu and M. Spiegel, *Corrosion Science* **49**, 2007 (1799).
18. B. Jönsson, R. Berglund, J. Magnusson, P. Henning and M. Hättestrand, *Materials Science Forum* **461–464**, 2004 (455).
19. H. Asteman, R. Norling, J. E. Svensson, A. Nylund and L. Nyborg, *Surface and Interface Analysis* **34**, 2002 (234).
20. C. W. F. T. Pistonius, *Zeitschrift für Physikalische Chemie* **35**, 1962 (109).
21. J. Engkvist, N. Israelsson and U. Bexell, *Surface and Interface Analysis* **45**, 2012 (445).
22. S. Canovic, J. Engkvist, F. Liu, H. Lai, H. Götlind, K. Hellström, J.-E. Svensson, L.-G. Johansso, M. Olsson and H. Halvarsson, *Journal of the Electrochemical Society* **157**, 2010 (C223).
23. F. H. Stott, G. C. Wood and J. Stringer, *Oxidation of metals* **44**, 1995 (113).
24. F. Liu, H. Götlind, J.-E. Svensson, L.-G. Johansson and M. Halvarsson, *Corrosion Science* **50**, 2008 (2272).
25. F. Liu, H. Josefsson, J. E. Svensson, L. G. Johansson and M. Halvarsson, *Materials at High Temperatures* **22**, 2005 (521).
26. A. Czyrska-Filemonowicz, K. Szot, A. Wasilkowska, A. Gil and W. J. Quadakkers, *Solid State Ionics* **117**, 1999 (13).
27. H. Götlind, F. Liu, J.-E. Svensson, M. Halvarsson and L.-G. Johansson, *Oxidation of metals* **67**, 2007 (251).
28. N. Israelsson, K. Hellström, J.-E. Svensson and L.-G. Johansso, KCl-induced corrosion of the FeCrAl alloy Kanthal ® AF at 600°C and the effect of H_2O, *Oxidation of Metals* (2014). doi:10.1007/s11085-014-9506-3.
29. J. Pettersson, J. E. Svensson and L. G. Johansson, *Oxidation of metals* **72**, 2009 (159).
30. FactSage 6.2 (Databases: Fact53, ELEM, BINS).